Journal of Thermal Engineering
Web page info: https://jten.yildiz.edu.tr
DOI: 10.18186/thermal.990615

Research Article

Impact of outer velocity on flow, heat and mass transfer of Casson nanofluid over a non-linear stretching sheet

Vinita MAKKAR[1], Vikas POPLY[1,*]

[1]Department of Basic and Applied Sciences, School of Engineering and Sciences, GD Goenka University, Gurgaon-, Haryana, India

ARTICLE INFO

Article history
Received: 04 January 2020
Accepted: 15 March 2020

Key words:
Non-linear stretching sheet; Brownian motion; Thermophoresis; Casson fluid; MHD

ABSTRACT

Steady boundary layer flow with Casson nanofluid in the presence of outer velocity towards a non-linear stretching sheet has been studied numerically. The main purpose of present study is to investigate the significance of various fluid parameters namely Casson fluid (non-Newtonian), thermophoresis, magnetic parameter, Brownian motion and non-linear stretching parameter on profiles of velocity, temperature and nanoparticle concentration. Non-linear governing equations and the linked boundary conditions are computed by shooting technique with the help of Runge Kutta Fehlberg (RKF) method by applying similarity conversions on it. The influence of various fluid parameters for different values of outer velocity on the rate of mass, heat and flow transportation are determined and represented through graphs and tables. The outcome reveals that with an increase in outer velocity, the velocity increases while temperature and concentration decreases. Present results of the study are correlated for $-\theta_0'(0)$ with the extant outcomes in literature as a limiting case in absence of thermophoresis parameter and Brownian motion. The present study finds utilization in industrial, biological, manufacturing as well as technological fields as these results are helpful for better controlling of heat transportation due to the presence of magnetic flow and outer velocity flow.

Cite this article as: Vinita V, Poply V. Impact of outer velocity on flow, heat and mass transfer of casson nanofluid over a non-linear stretching sheet. J Ther Eng 2021;7(6):1353−1365.

INTRODUCTION

Flow behavior over stretching surfaces has attracted many authors due to its wide area of industrial and manufacturing applications like artificial fibers, manufacturing of metallic sheets, petroleum industries, metal spinning, polymer processing etc. The flow caused by the stretching surface was initially investigated by Crane [1]. After that, Gupta and Gupta [2] and Dutta et al. [3] gained new heights of Crane [1] work by comprising the analysis of mass and heat transportation using many different aspects. Yoon et al. [4] reported the comparison between theoretical and experimental results by considering a thin metal stretching

***Corresponding author.**
*E-mail address: vini252011makkar@gmail.com, vikaspoply@gmail.com

This paper was recommended for publication in revised form by Regional Editor Regional Editor Baha Zafer

sheet. Sarma and Rao [5] investigated the flow behavior in viscoelastic fluid over a stretching sheet. The nanofluid also comes in existence when we add a small quantity of nano-sized particles which are also called ultrafine particles to the base fluid. Recently, study of nanofluid has much more importance due to its uses, properties and applications in different research areas. Choi and Eastman [6] introduced the concept of nanofluid. The main characteristic of nanofluid is to increase the thermal conductivity of base fluid [7].

In recent years, MHD flow has gained attention due to its controllable heat transfer rate and great utilizations in various industrial areas and manufacturing processes. Hayat et al. [8] studied the impact of MHD on heat and flow transportation over stretching surfaces. On stretching surfaces, a stagnation point micropolar MHD nanofluid flow was numerically investigated by Anwar et al. [9]. After that Shawky et al. [10] studied Williamson nanofluid towards a stretching sheet and he reported that the increment in non-Newtonian parameter increases both the Skin friction coefficient as well as the rate of heat transfer. Vajravelu and Cannon [11] examined the flow behavior of fluid on non-linear stretching sheet. Also, a mixed convection magnetohydrodynamic nanofluid flow along with entropy analysis on a non-linear stretching sheet has been represented by Matin et al. [12]. Das [13] studied the partial slip effect on nanofluid past a permeable non-linearly stretching sheet. Powell-Eyring MHD nanofluid flow having variable thickness past a non-linear stretched surface was interpreted by Hayat et al. [14]. Jain and Choudhary [15] investigated the Soret and Dufour effects with MHD flow using chemical reactions. Siddheshwar and Mahabaleshwar [16] studied the problem of heat and flow transportation on non-linear stretching sheet with suction/injection.

The yield stress is displayed by a non-Newtonian Casson fluid. Fluid acts as a solid, if the yield stress is more than the applied shear stress. On the other hand, fluid behaves as a liquid if the yield stress is less than the applied shear stress. Recently, Casson fluid has gained more attention due to its vast applications and uses in many industrial and medical sectors [17]. Nadeem et al. [18] analyzed the effect of MHD flow in Casson fluid over a porous stretching sheet. Kameswaran et al. [19] investigated the dual solution in a Casson fluid flow past a shrinking/stretching sheet. Krishna et al. [20] studied the chemical reaction effect on MHD Casson fluid flow taking porous medium on a stretched surface. Hakeem et al. [21] used impermeable stretching surface with Casson fluid to determine the inclined Lorentz force effect on heat and flow transportation. Murthy [22] investigated the unsteady MHD Casson fluid flow with partial slip on exponentially stretching sheet. Recently, various aspects on the rate of flow, heat and mass characteristics are analyzed by numerous authors in [23]–[29].

Furthermore, the non-linear effect over stretching surfaces under different physical circumstances has also been examined by researchers in [30]–[35]. No study has been done so far to analyze the combined effect of outer velocity with non-linear stretching in a Casson nanofluid. In present study, we analyzed the combined effect of outer velocity with non-linear stretching sheet in a MHD Casson nanofluid. In this analysis, we observe that an inverted boundary layer is formed in velocity profiles when we take the outer velocity parameter greater than one. Also, outer velocity has a great impact on the rate of heat transportation and nanoparticle concentration. The outcomes of Current study reveals that as non-linearity in the stretching sheet increases, velocity decreases for outer velocity less than one and increases for outer velocity greater than one.

MATERIALS AND METHODS

2-D incompressible boundary layer flow with Casson nanofluid towards a non-linear stretching sheet has been considered. This non-linear behavior produces a flow and sheet is stretched with stretching velocity $u_w = ax^N$, where a, x and N denotes a constant, stretching surface coordinate and non-linear stretching parameter respectively. Figure 1 depicts the physical model of the present problem. In this physical configuration system, T_w, C_w, T_∞ and C_∞ represents temperature at the sheet, nanoparticle volume fraction at surface, ambient temperature attained and ambient nanoparticle volume fraction serially. The induced magnetic field is very small comparative to apply magnetic field so is neglected. The basic governing equations for nanofluid in terms of Cartesian coordinates are described as:

$$\frac{\partial u}{\partial x}+\frac{\partial u}{\partial y}=0 \tag{1}$$

$$u\frac{\partial u}{\partial x}+v\frac{\partial u}{\partial y}=U\frac{\partial U}{\partial x}+\nu\left(1+\frac{1}{\beta}\right)\frac{\partial^2 u}{\partial y^2}-\frac{\sigma B^2}{\rho}\left(u-U\right) \tag{2}$$

$$u\frac{\partial T}{\partial x}+v\frac{\partial T}{\partial y}=\alpha_m\nabla^2 T+\tau\left[D_B\frac{\partial C}{\partial y}\frac{\partial T}{\partial y}+\left(D_T/T_\infty\right)\left(\frac{\partial T}{\partial y}\right)^2\right] \tag{3}$$

$$u\frac{\partial C}{\partial x}+v\frac{\partial C}{\partial y}=D_B\frac{\partial^2 C}{\partial y^2}+\left(D_T/T_\infty\right)\frac{\partial^2 T}{\partial y^2} \tag{4}$$

Initial boundary conditions are given as:

$$\begin{aligned} &v=0,\ u_w=ax^N,\ C=C_w,\ T=T_w \text{ at } y=0\\ &u\to U=bx^N,\ C\to C_\infty,\ T\to T_\infty \text{ as } y\to\infty \end{aligned} \tag{5}$$

Here vertical and horizontal velocities are represented by v and u, respectively. Also ν, β, σ, B, ρ_f, U denotes the

kinematic viscosity, Casson fluid parameter, velocity slip parameter, magnetic field intensity, density of base fluid, outer velocity, $\alpha_m = \frac{k_m}{(\rho c)_f}$ is the thermal diffusivity, α is a positive constant, $\tau = \frac{(\rho c)_p}{(\rho c)_f}$ defines a proportion of heat capacities of nanofluid to base fluid, ρ_p is density of particles, D_T is thermophoretic diffusion coefficient and D_B is Brownian diffusion coefficient.

Equations (1) to (4) with boundary conditions (5) are transformed using similarity variables

$$\begin{aligned}
&\xi = y\sqrt{\frac{a(N+1)}{2\nu}}x^{\frac{N-1}{2}}, u = ax^N f_0'(\xi),\\
&v = -\sqrt{\frac{a(N+1)}{2}}x^{\frac{N-1}{2}}\left(f_0(\xi)+\left(\frac{N-1}{N+1}\right)\xi f_0'(\xi)\right)\\
&\theta_0(\xi) = \frac{T-T_\infty}{T_w-T_\infty}, \phi_0(\xi) = \frac{C-C_\infty}{C_w-C_\infty}
\end{aligned} \tag{6}$$

Substituting equation (6) into equations (2) to (4), we have

$$\begin{aligned}
&\left(1+\frac{1}{\beta}\right)f_0''' + f_0 f_0'' - \left(\frac{2N}{N+1}\right)\left(f_0'^2-\lambda^2\right)f_0'^2\\
&-\left(\frac{2}{N+1}\right)M\left(f_0'-\lambda\right) = 0
\end{aligned} \tag{7}$$

$$\frac{1}{\Pr}\theta_0' + f_0\theta_0' + Nb\theta_0'\phi_0' + Nt\theta_o'^2 = 0 \tag{8}$$

$$\phi_0'' + \frac{1}{2}Scf_0\phi_O' + \frac{Nt}{Nb}\theta_O'' = 0 \tag{9}$$

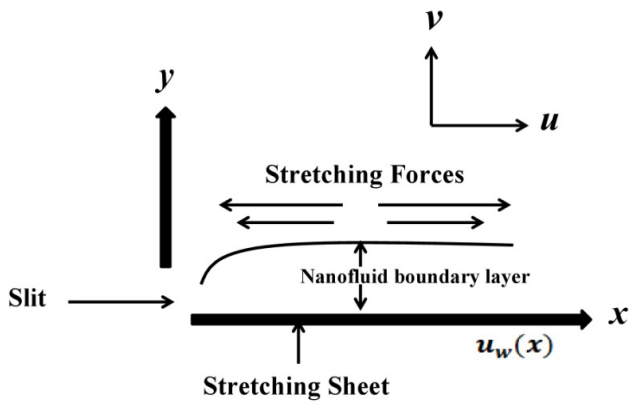

Figure 1. Physical model of problem.

The transformed boundary conditions are

$$\begin{aligned}
&f_0(0) = 0,\ f_0'(0) = 1,\ \phi_0(0) = 1,\ \theta_0(0) = 1\\
&\text{and } f_0'(\xi) \to \lambda,\ \phi_0(\xi) \to 0,\ \theta_0(\xi) \to 0 \text{ as } \xi \to \infty
\end{aligned} \tag{10}$$

where $(\,)'$ denotes derivative w.r.t ξ. Here λ, M, Nt, Nb, Sc and Pr represents the outer velocity parameter, magnetic parameter, thermophoresis parameter, Brownian motion parameter, Schmidt number and Prandtl number respectively and these fluid parameters are given by:

$$\begin{aligned}
&\lambda = \frac{b}{a}, M = \frac{\sigma B^2}{ax^{N-1}}, Nt = \frac{(\rho c)_p D_T (T_w - T_\infty)}{(\rho c)_f T_\infty \nu},\\
&Nb = \frac{(\rho c)_p D_B (C_w - C_\infty)}{(\rho c)_f \nu}, Sc = \frac{\nu}{D_B} \text{and } Pr = \frac{\nu}{\alpha}
\end{aligned} \tag{11}$$

Also, local Sheerwood number and local Nusselt number are respectively defined as:

$$Sh_x = \frac{xq_m}{D_B(C_w - C_\infty)} \text{ and } Nu_x = \frac{xq_w}{k(T_f - T_\infty)} \tag{12}$$

where q_m and q_w are mass flux and heat flux at the stretching surface serially

$$q_m = -D_B(C_w - C_\infty)x^{\frac{N-1}{2}}\sqrt{\frac{a(N+1)}{2\nu}}\phi_0'(0) \tag{13}$$

$$q_w = -k(T_w - T_\infty)x^{\frac{N-1}{2}}\sqrt{\frac{a(N+1)}{2\nu}}\theta_0'(0) \tag{14}$$

NUMERICAL PROCEDURE

The system of non-linear differential equations (7)–(9) are not solved analytically due to extremely non-linear behaviour. To solve this system of non-linear differential equations (7)–(9) together with boundary conditions (10), we adopt Runge Kutta Fehlberg approach (numerical procedure) with shooting technique. The coupled differential equations (7)–(9) has been reduced to a system of first order differential equations and are described as:

$$y_1' = y_2 \tag{15}$$

$$y_2' = y_3 \tag{16}$$

$$y_3' = \frac{1}{\left(1+\frac{1}{\beta}\right)}\left[-y_1 y_3 + \frac{2}{N+1}M\left(y_2^2-\lambda^2\right) + \frac{2}{N+1}M\left(y_2-\lambda\right)\right] \tag{17}$$

$$y_4' = y_5 \tag{18}$$

$$y_5' = -Pr\left[y_1 y_5 + Nby_5 y_7 + Nty_5^2 \right] \quad (19)$$

$$y_6' = y_7 \quad (20)$$

$$y_7' = -\frac{1}{2} y_1 y_7 Sc + \frac{Nt}{Nb} Pr\left[y_1 y_5 + Nby_5 y_7 + Nty_5^2 \right] \quad (21)$$

The relevant boundary conditions are reduced to

$$\begin{aligned} &y_1 = 0, y_2 = 1, y_6 = 1, y_4 = 1 \text{ at } \xi = 0 \\ &\text{and } y_2 = \lambda, y_6 = 0, y_4 = 0 \text{ as } \xi \to \infty \end{aligned} \quad (22)$$

Where

$$\begin{aligned} y_1 = f_0, y_2 = f_0', y_3 = f_0'', y_3' = f_0''' \\ y_4 = \theta_0, y_5 = \theta_0', y_5' = \theta_0'' \\ y_6 = \phi_0, y_7 = \phi_0', y_7' = \phi_0'' \end{aligned} \quad (23)$$

The above system of differential equations is solved using shooting technique with RKF method. Figure 2 display the flow chart of numerical procedure adopted above.

RESULTS AND DISCUSSION

In current study, non-linear differential equations (7)–(9) with boundary conditions (10) are computed numerically. The variation of fluid parameters like magnetic parameter *M*, Prandtl number *Pr*, thermophoresis parameter *Nt*, Brownian motion parameter *Nb*, Schmidt number *Sc*, non-linear stretching parameter *N* and Casson fluid parameter β on velocity distribution, fluid temperature and nanoparticle concentration are computed and explained through graphs and tables.

Table 1 represents the validation of our outcomes for $-\theta_0'(0)$ with $Nb = 0$, $Nt = 0$ and for various entries of *N* and *Pr*. In present problem, an excellent validation of the numerical procedure are done with those of Rana and Bhargava [33]

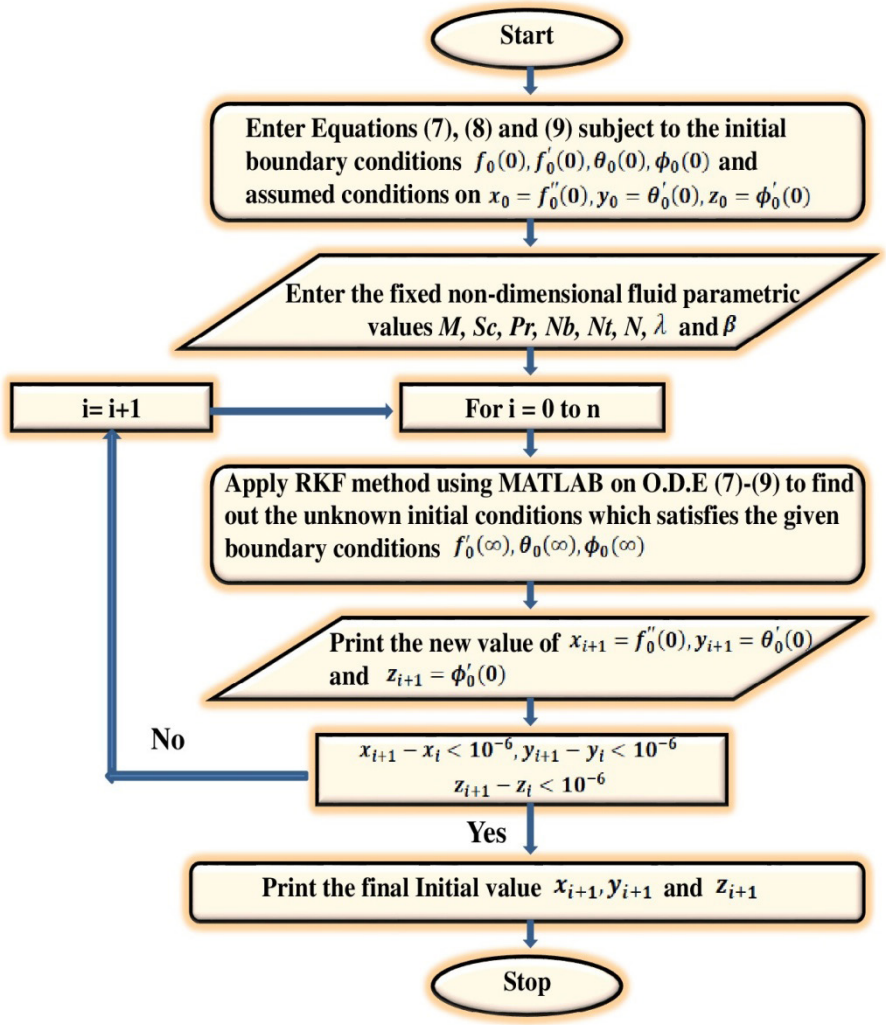

Figure 2. Flow chart of Numerical procedure.

Table 1. Values of $-\theta_0'(0)$ with $Nb = 0$ and $Nt = 0$, a comparison

Pr	*N*	Rana and Bhargava [33]	Cortell [32]	Present results
1.0	0.1	0.6101	0.6102	0.6102
	0.5	0.5955	0.5952	0.5952
	1.5	0.5756	0.5745	0.5747
	3.0	0.5660	0.5644	0.5647
5.0	0.1	1.5683	1.6071	1.6077
	0.5	1.5512	1.5867	1.5867
	1.5	1.5269	1.5574	1.5576
	3.0	1.5144	1.5423	1.5431

and Cortell [32] by neglecting the entries of *Nt* and *Nb*. Table 2 shows the influence of various fluid parameters Schmidt number *Sc*, magnetic field parameter *M*, Prandtl number *Pr*, Brownian motion parameter *Nb*, thermophoresis parameter *Nt*, non-linear stretching parameter *N* and Casson fluid parameter β on velocity, temperature and concentration for two distinct values of outer velocity λ.

Figures 3 and 4 show the effect of β on velocity profiles for $\lambda = 0.5$ and $\lambda = 1.2$ respectively. As Casson parameter β increases, fluid yield stress decreases that hurdles the free movement of fluid particles and consequently width of boundary layer decreases that will declines the fluid velocity for $\lambda = 0.5$ as shown in Figure 3. Thusly, Skin friction coefficient exceeds for large values of β as computed in Table 2. On contrary, inverse trend is observed in case of $\lambda = 1.2$ that can be seen in Figure 4.

Further, the impact of Casson fluid parameter β on fluid temperature and nanoparticle concentration is depicted in Figures 5–8. Figures 5 and 6 represents the temperature profile for two distinct values of outer velocity λ (i.e. for $\lambda = 0.5$ and $\lambda = 1.2$). With an increase in the value of Casson fluid parameter β, fluid velocity goes on decreasing for $\lambda = 0.5$ that will decrease the rate of heat transfer and thus fluid

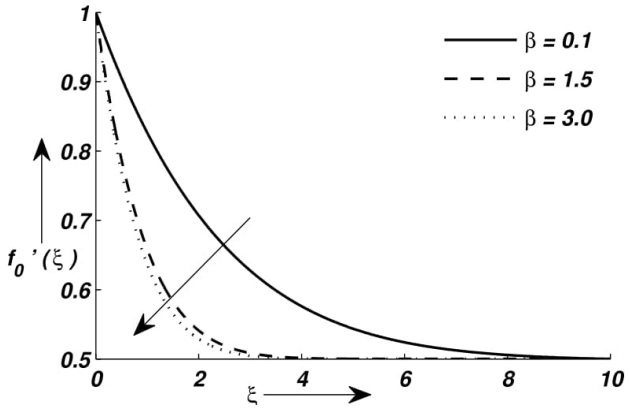

Figure 3. Impact of Casson fluid parameter β on velocity profile $f_0'(\xi)$, when $\lambda = 0.5$.

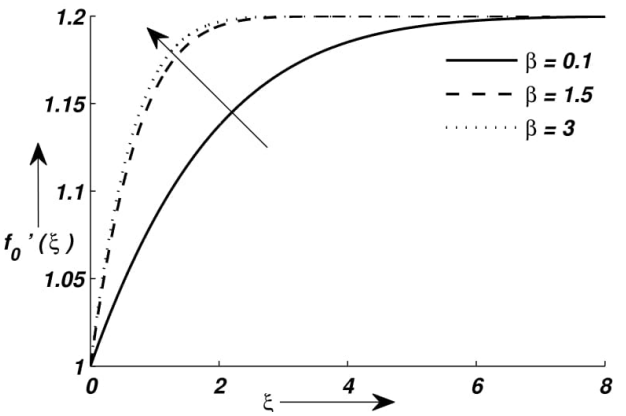

Figure 4. Impact of Casson fluid parameter β on velocity profile $f_0'(\xi)$, when $\lambda = 1.2$.

temperature enhances for $\lambda = 0.5$ that can be visualized in Figures 5. Hence, Nusselt number declines for larger values of β can be seen in Table 2. Also, a very small decrease in fluid temperature is noticed for $\lambda = 1.2$ as seen in Figure 6. Figures 7 and 8 display the impact of Casson fluid parameter β on nanoparticle concentration for $\lambda = 0.5$ and $\lambda = 1.2$ respectively. Figure 7 shows that an intensification in the value of β results to increase the nanoparticle concentration for outer velocity $\lambda = 0.5$ which increase the value of local Sheerwood number. On the other hand, reverse trend is observed for nanoparticle concentration when $\lambda = 1.2$ as visualized in Figure 8.

Also, Figures 9 and 10 demonstrate the temperature profiles for various values of Schmidt number *Sc*. With an increase in the values of *Sc*, thermal diffusivity enhances which results in increase in the thickness of boundary layer and therefore fluid temperature increases for both values of λ and thusly, Nusselt number decreases that can be seen from Table 2. Furthermore, Figures 11 and 12 represents the effect of *Sc* on nanoparticle concentration for $\lambda = 0.5$ and $\lambda = 1.2$ respectively. As *Sc* increases, mass diffusivity decreases. Thus, nanoparticle concentration reduces as illustrated in the Figures 11 and 12 for both $\lambda = 0.5$ and $\lambda = 1.2$ respectively.

Figures 13 and 14 depicts the variation in velocity distribution under the influence of magnetic parameter *M* for two distinct cases of outer velocity $\lambda = 0.5$ and $\lambda = 1.2$ respectively. Here, the presence of *M* will generates Lorentz force which hurdles the free movement of fluid particles. Thus magnetism can be used to control the velocity of nanofluid flow over stretching sheet. An increase in the value of *M* causes the declination of nanofluid velocity shown in Figure 13. Whereas reverse nature is observed for $\lambda = 1.2$ as shown in Figure 14 due to an inverted boundary layer formation for $\lambda > 1$. Figure 15 demonstrate variation of magnetic parameter *M* on temperature field for $\lambda = 0.5$. From Figure 15, it is clear that an enlargement in magnetic

Table 2. Results of $f_0''(0)$, $-\theta_0'(0)$ and $-\phi_0'(0)$ for distinct fluid parameters when $\lambda = 0.5$ and $\lambda = 1.2$

Sc	*M*	*Nb*	*Nt*	*N*	*β*	$\lambda = 0.5$			$\lambda = 1.2$		
						$f_0''(0)$	$-\theta_0'(0)$	$-\phi_0'(0)$	$f_0''(0)$	$-\theta_0'(0)$	$-\phi_0'(0)$
1	0.1	0.1	0.3	1	0.1	−0.20677	1.23789	−2.08444	0.10357	1.24931	−1.90466
1.5						−0.20677	1.15700	−1.55004	0.10357	1.17005	−1.37031
2						−0.20677	1.09805	−1.14784	0.10357	1.11254	−0.96987
1	0.1					−0.20677	1.23789	−2.08444	0.10357	1.24931	−1.90466
	2.5					−0.31125	1.23115	−2.11876	0.13920	1.25211	−1.90099
	5.0					−0.39190	1.22494	−2.13539	0.16863	1.25449	−1.89970
	0.1	0.1				−0.20677	1.23789	−2.08444	0.10357	1.24931	−1.90466
		0.2				−0.20677	1.10864	−0.59558	0.10357	1.11078	−0.46481
		0.3				−0.20677	0.98758	−0.10767	0.10357	0.98186	−0.00532
		0.1	0.1			−0.20677	1.46024	−0.55665	0.10357	1.49450	−0.48140
			0.3			−0.20677	1.23789	−2.08444	0.10357	1.24931	−1.90466
			0.5			−0.20677	1.04362	−2.90754	0.10357	1.03730	−2.56204
			0.3	0.1		−0.14406	1.24148	−2.05988	0.06685	1.24661	−1.91194
				1		−0.20677	1.23789	−2.08444	0.10357	1.24931	−1.90466
				10		−0.25560	1.23476	−2.10018	0.13082	1.25144	−1.90149
				1	0.1	−0.20677	1.23789	−2.08444	0.10357	1.24931	−1.90466
					1.5	−0.53094	1.21311	−2.16074	0.26608	1.26267	−1.89896
					3.0	−0.59361	1.20683	−2.16097	0.29749	1.26529	−1.90154

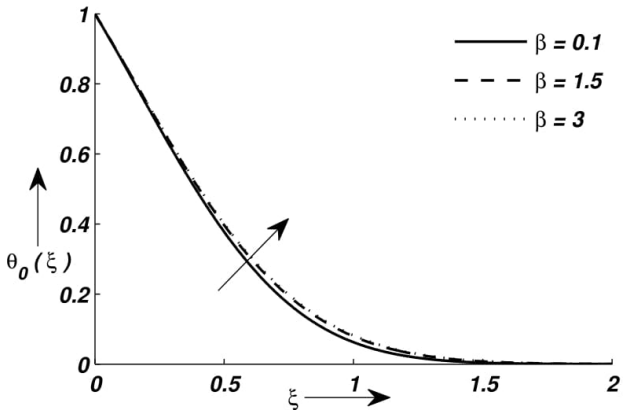

Figure 5. Impact of Casson fluid parameter β on temperature profile $\theta_0(\xi)$, when $\lambda = 0.5$.

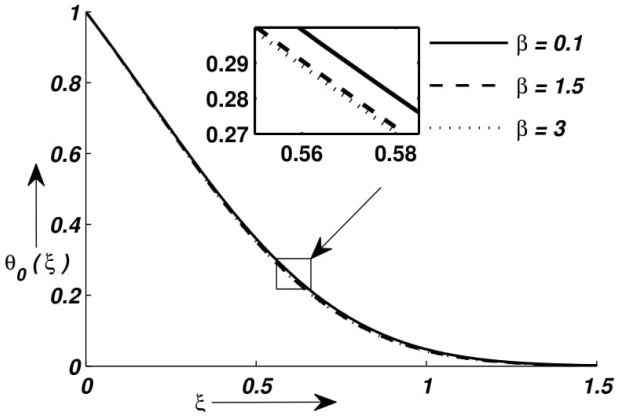

Figure 6. Impact of Casson fluid parameter β on temperature profile $\theta_0(\xi)$, when $\lambda = 1.2$.

field produces a slight enhancement in fluid temperature for $\lambda = 0.5$. After that, Figure 16 expresses the variation in nanoparticle concentration with change in the value of *M*. For larger value of magnetic parameter *M* nanoparticle concentration increases for $\lambda = 0.5$ as represented in Figure 16. Physically, this can be explained that as *M* increases, fluid velocity decreases due to this rate of mass transfer decreases and hence concentration increases. Also from Table 2, we observed that as *M* increases, Sheerwood number decreases which represent the reduction in the convective mass transfer and hence concentration increases.

Impact of non-linear stretching parameter *N* on profiles of velocity, temperature and concentration for different values of outer velocity are represented by the Figures 17–22. With an increase in the value of non-linear stretching parameter *N* fluid velocity decreases (as shown in Figure 17 for $\lambda < 1$ and increases for $\lambda > 1$ due to invested boundary layers formations as seen in Figure 18. Consequently, momentum boundary layer thickness decreases with increasing non-linear stretching parameter *N* for both values of λ. Thus, the presence of nonlinear stretching parameter leads to slight rise the thickness of thermal boundary

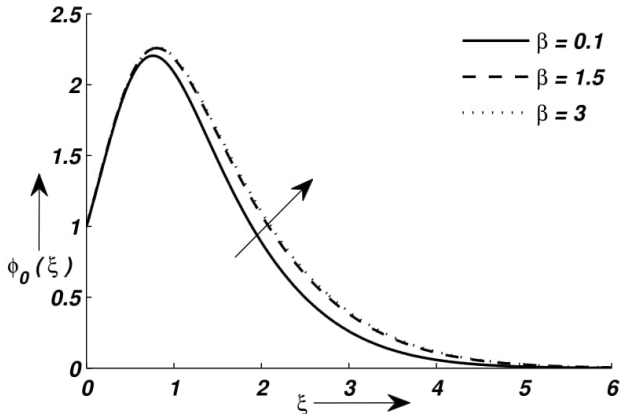

Figure 7. Impact of Casson fluid parameter β on concentration profile $\phi_0(\xi)$, when $\lambda = 0.5$.

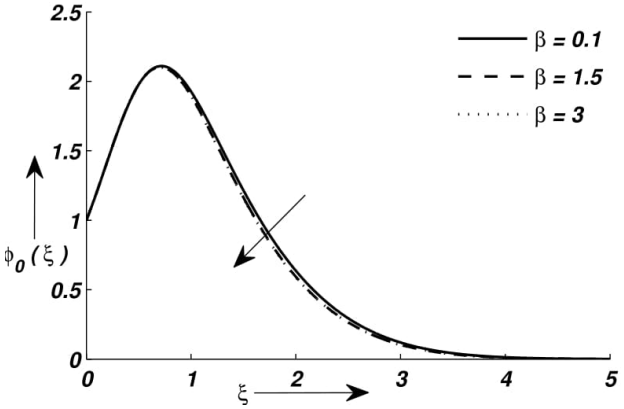

Figure 8. Impact of Casson fluid parameter β on concentration profile $\phi_0(\xi)$, when $\lambda = 1.2$.

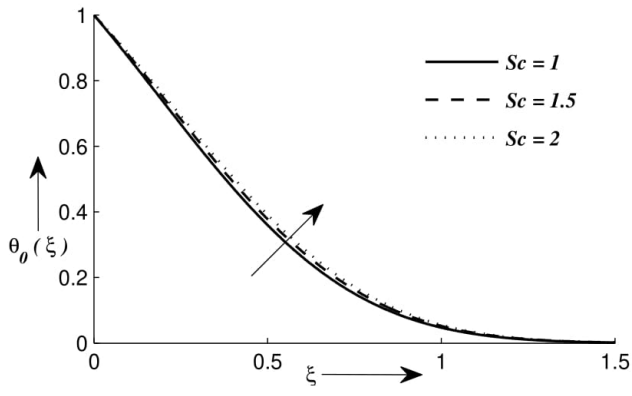

Figure 9. Impact of Schmidt number *Sc* on temperature profile $\theta_0(\xi)$, when $\lambda = 0.5$.

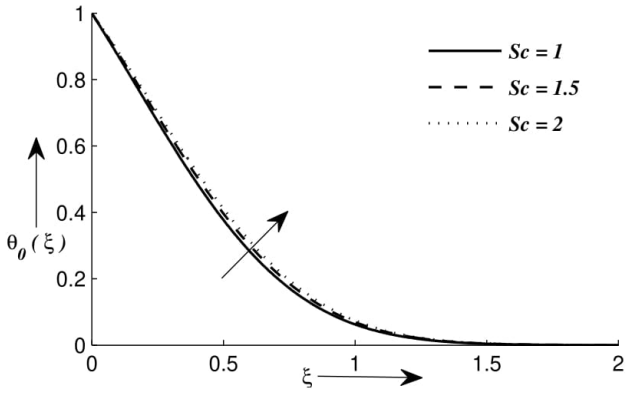

Figure 10. Impact of Schmidt number *Sc* on temperature profile $\theta_0(\xi)$, when $\lambda = 1.2$.

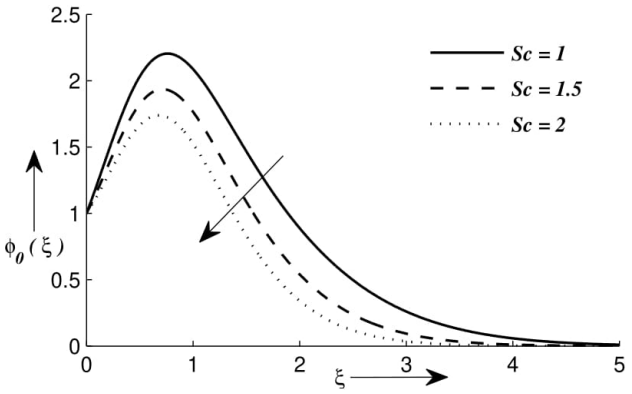

Figure 11. Impact of Schmidt number *Sc* on concentration profile $\theta_0(\xi)$, when $\lambda = 0.5$.

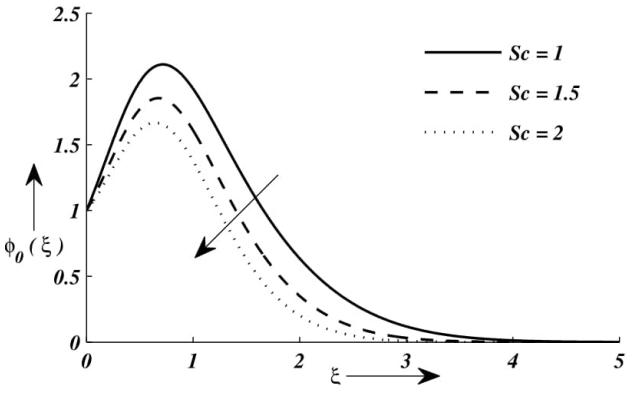

Figure 12. Impact of Schmidt number *Sc* on concentration profile $\theta_0(\xi)$, when $\lambda = 1.2$.

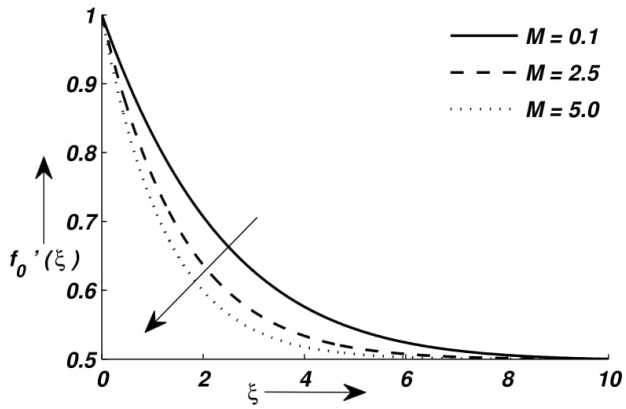

Figure 13. Impact of magnetic parameter M on velocity profile $f'_0(\xi)$, when $\lambda = 0.5$.

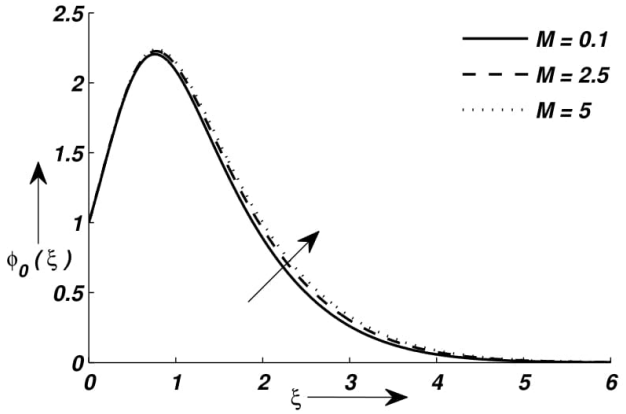

Figure 16. Impact of magnetic parameter M on temperature profile $\phi_0(\xi)$, when $\lambda = 1.2$.

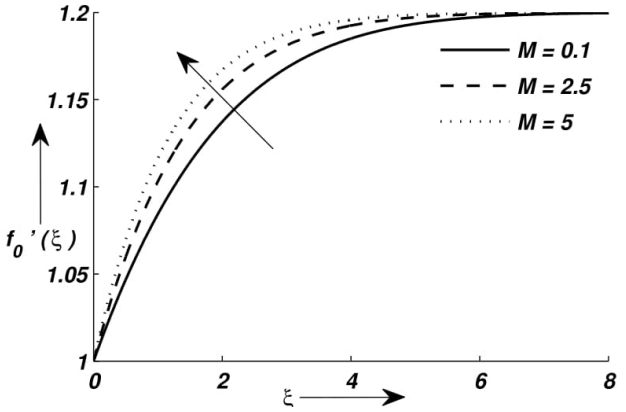

Figure 14. Impact of magnetic parameter M on velocity profile $f'_0(\xi)$, when $\lambda = 1.2$.

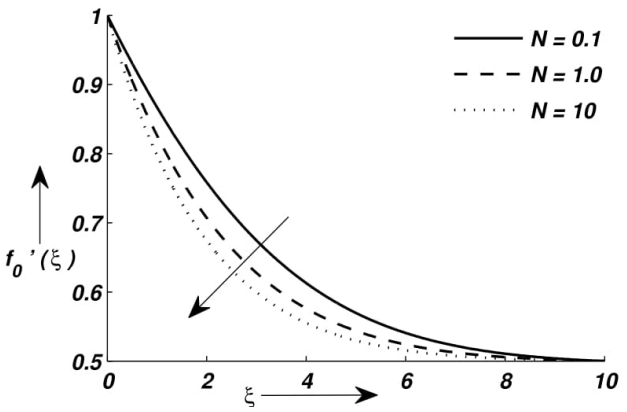

Figure 17. Impact of non-linear stretching parameter N on velocity profile $f'_0(\xi)$, when $\lambda = 0.5$.

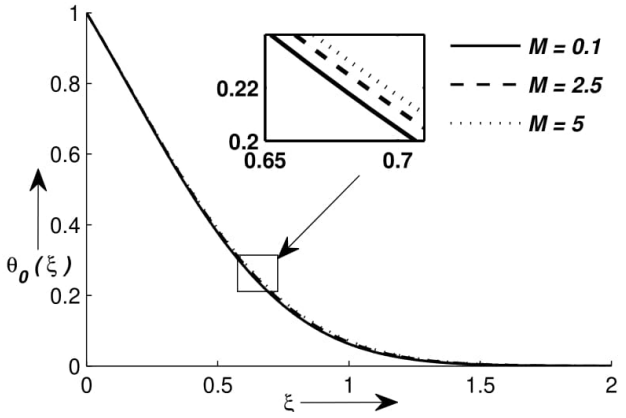

Figure 15. Impact of magnetic parameter M on temperature profile $\theta_0(\xi)$, when $\lambda = 0.5$.

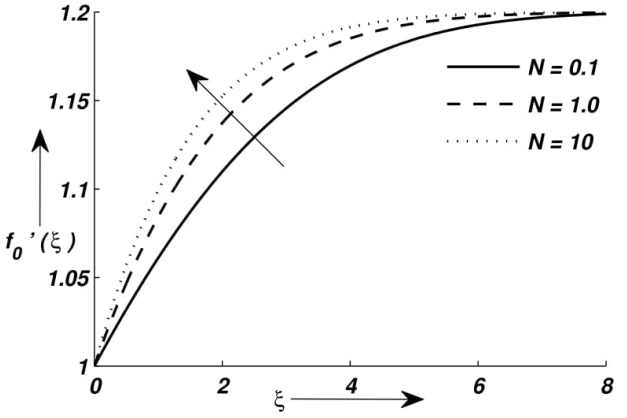

Figure 18. Impact of non-linear stretching parameter N on velocity profile $f'_0(\xi)$, when $\lambda = 1.2$.

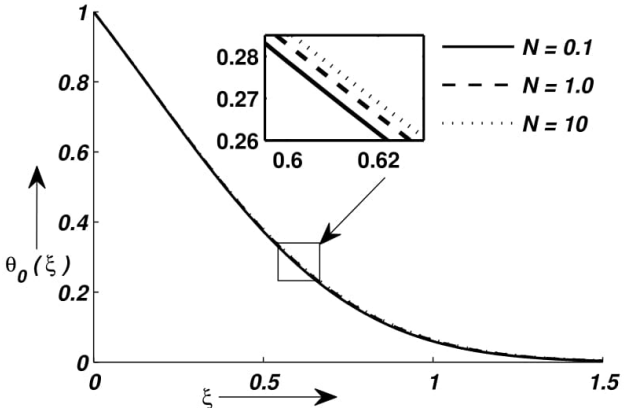

Figure 19. Impact of non-linear stretching parameter N on temperature profile $\theta_0(\xi)$, when $\lambda = 0.5$.

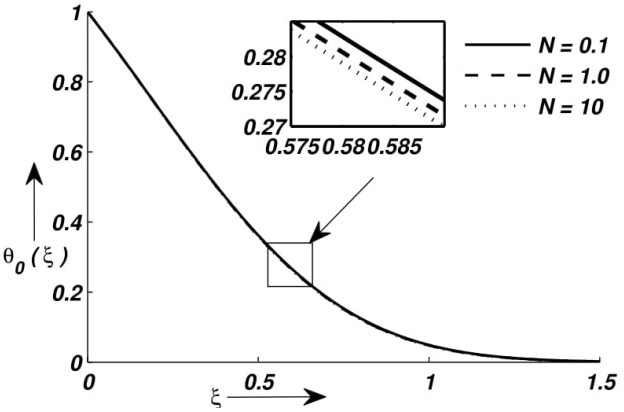

Figure 20. Impact of non-linear stretching parameter N on temperature profile $\theta_0(\xi)$, when $\lambda = 1.2$.

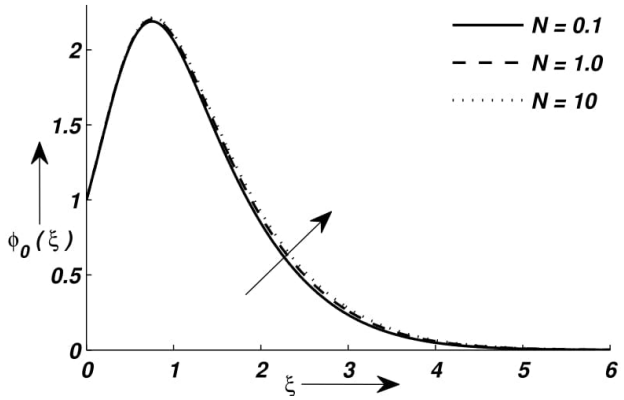

Figure 21. Impact of non-linear stretching parameter N on temperature profile $\phi_0(\xi)$, when $\lambda = 0.5$.

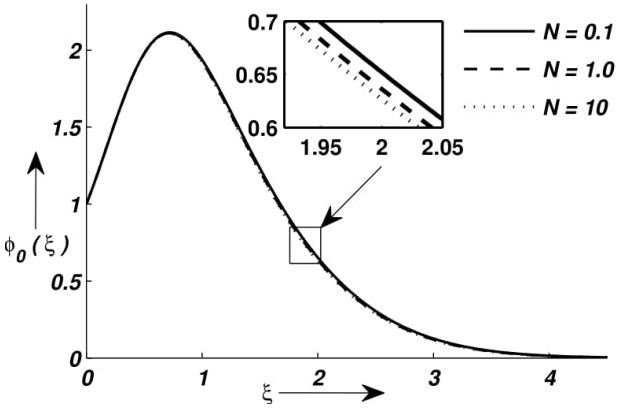

Figure 22. Impact of non-linear stretching parameter N on temperature profile $\phi_0(\xi)$, when $\lambda = 1.2$.

layer and hence fluid temperature increases slightly for $\lambda < 1$ as shown in Figure 19. On the other hand, reverse impact is noticed for outer velocity parameter greater than one as visualized in Figure 20. Due to the presence of outer velocity, the variation in the temperature profile are less as shown in Figure 19 and 20. The impacts of non-linear stretching parameter N on profiles of nanoparticle concentration are represented by Figures 21 and 22 for two cases of λ. As N increases, nanoparticle concentration increases for $\lambda < 1$ and decreases for $\lambda > 1$ as depicted in Figures 21 and 22.

Figures 23 and 24 demonstrate the impact on fluid temperature for $\lambda = 0.5$ and $\lambda = 1.2$ with variation of Brownian motion parameter Nb. A casual movement of suspended particles is the Brownian motion which comes to be in existence when liquid elements strike one another and that results an increase in temperature at the surface as seen in Figures 23 and 24 for both cases of λ. The striking of atoms or molecules of the fluid particles with each other will create an arbitrary motion called Brownian motion of suspended (Pendolus) particles and that will enhance the width of boundary layer. Consequently, for larger Nb, temperature gradient falls as visualized in Table 2. A small increment is noticed in case of temperature profile for higher values of Nb. An impact of Nb on $\phi_0(\xi)$ for various values of λ is represented by the Figures 25 and 26. Higher value Nb of will increase the fluid particles collision by which nanoparticle concentration declines for considered cases of λ.

Table 3 represents the impact of outer velocity parameter λ on velocity profile $f_0''(0)$, temperature profile $-\theta_0'(0)$ and concentration profile $-\phi_0'(0)$ by taking fixed entries of fluid parameters as $M = 0.1$, $Pr = 5$, $Nb = 0.1$, $Nt = 0.3$, $Sc = 1$, $N = 1$ and $\beta = 0.1$. Here, it is observed that velocity profile increases and consequently, Skin friction coefficient increases. Intensification in the value of outer velocity λ causes the value of fluid temperature as well as nanoparticle concentration to declines and their respective local Nusselt number and local Sheerwood number increases.

Also, Figures 27 and 28 depicts the fluid temperature under the influence of thermophoresis parameter Nt for $\lambda = 0.5$ and $\lambda = 1.2$. Consequently, temperature gradient falls

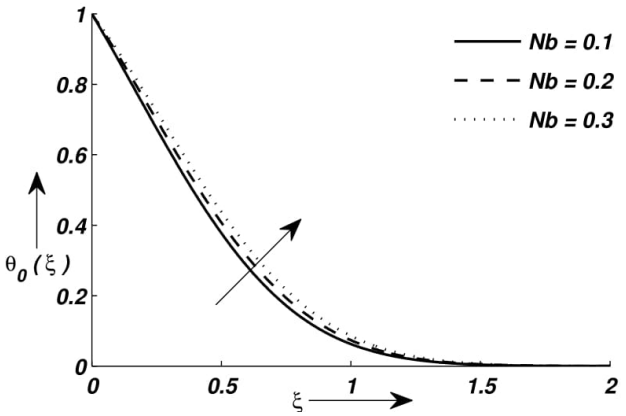

Figure 23. Impact of Brownian motion parameter *Nb* on temperature profile $\theta_0(\xi)$, when $\lambda = 0.5$.

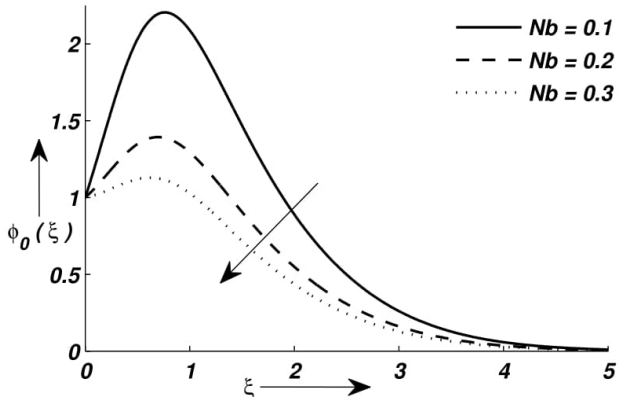

Figure 25. Impact of Brownian motion parameter *Nb* on concentration profile $\phi_0(\xi)$, when $\lambda = 0.5$.

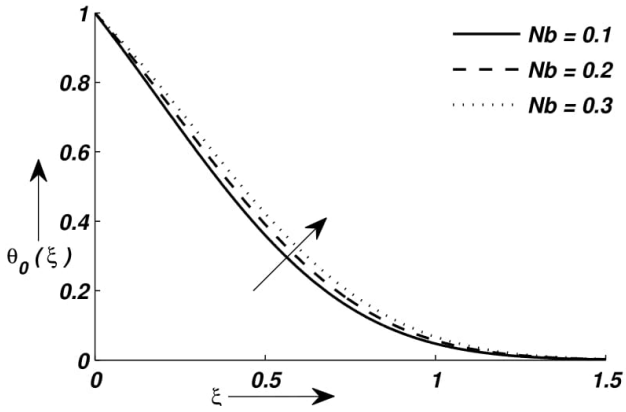

Figure 24. Impact of Brownian motion parameter *Nb* on temperature profile $\theta_0(\xi)$, when $\lambda = 1.2$.

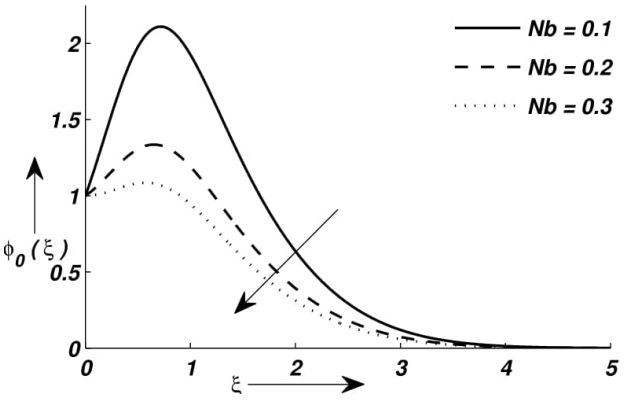

Figure 26. Impact of Brownian motion parameter *Nb* on concentration profile $\phi_0(\xi)$, when $\lambda = 1.2$.

Table 3. Values of $f_0''(0)$, $-\theta_0'(0)$ and $-\phi_0'(0)$ for different λ with fixed entries of various fluid parameters as $M = 0.1$, $Pr = 5$, $Nb = 0.1$, $Nt = 0.3$, $Sc = 1$, $N = 1$ and $\beta = 0.1$

λ	$f_0''(0)$	$-\theta_0'(0)$	$-\phi_0'(0)$
0.5	−0.20677	1.23789	−2.08444
0.8	−0.09223	1.24038	−2.00173
1.2	0.10357	1.24931	−1.90466

for larger value of *Nt* and that will decline the conduction of nanoparticles. Thus, ultrafine particles reallocate from warmer to colder place that ultimately raise the boundary layer thickness and thereby temperature goes high for both values of λ. Hence, Nusselt number comes down that can be visualized in Table 2. On the other hand, Figures 29 and 30 illustrate nanoparticle concentration for different λ under the consequence of *Nt* and simultaneously nanoparticle volume fraction field shows similar effect as that in case of temperature for each λ.

CONCLUSION

This study represents influence of outer velocity with mass and heat transportation on Casson nanofluid past a nonlinear stretching sheet. Present results are compared with Rana and Bhargava [33] and Cortell [32] as a limiting case of our study. Basic equations are solved by applying shooting technique. Main fallout of the present study incorporates the significance of non-linear stretching parameter and outer velocity in addition to MHD on profile of velocity, fluid temperature and nanoparticle concentration of heat, mass and flow transportation of Casson nanofluid. Key findings of current analysis for two distinct entries of outer velocity λ (i.e. $\lambda = 0.5$ and $\lambda = 1.2$) are summarized as:

1. For $\lambda = 0.5$; it is observed that velocity profile decreases for increasing value of non-linear stretching parameter *N*, Casson parameter β,

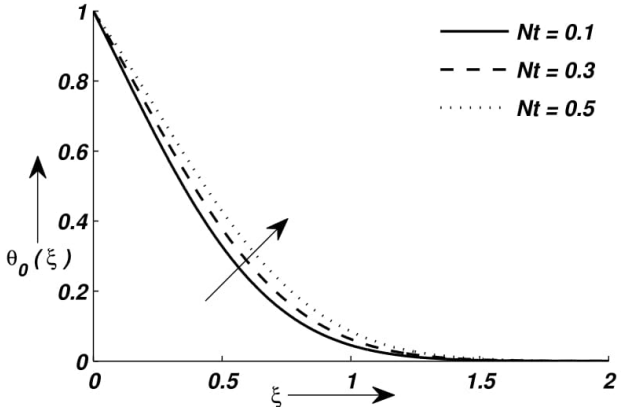

Figure 27. Impact of Brownian motion parameter *Nt* on temperature profile $\theta_0(\xi)$, when $\lambda = 0.5$.

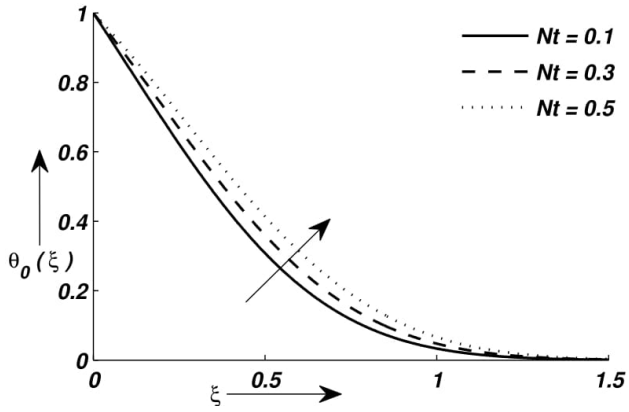

Figure 28. Impact of Brownian motion parameter *Nt* on temperature profile $\theta_0(\xi)$, when $\lambda = 1.2$.

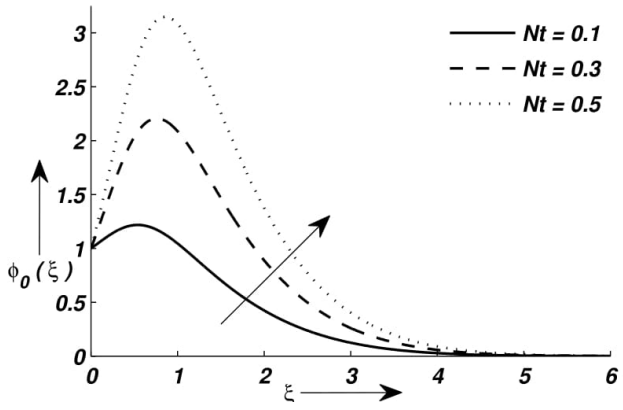

Figure 29. Impact of Brownian motion parameter *Nt* on concentration profile $\phi_0(\xi)$, when $\lambda = 0.5$.

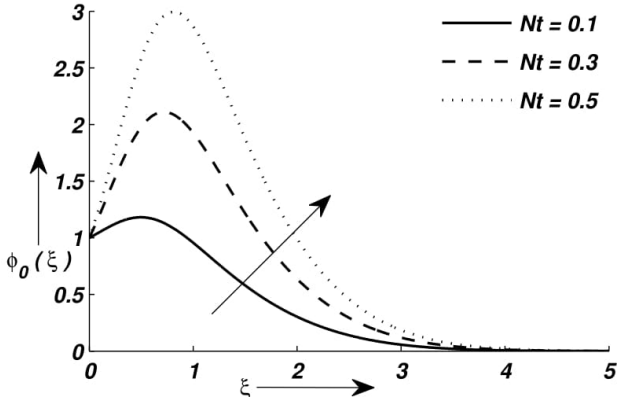

Figure 30. Impact of Brownian motion parameter *Nt* on concentration profile $\phi_0(\xi)$, when $\lambda = 1.2$.

and magnetic parameter *M*. Raise in temperature is noticed for Schmidt number *Sc*, Casson fluid parameter β, magnetic parameter *M*, non-linear stretching *N*, Brownian motion parameter *Nb* and thermophoresis parameter *Nt*. Also, nanoparticle concentration increases for Casson fluid parameter β, magnetic parameter *M*, non linear stretching parameter *N* and thermophoresis parameter *Nt* whereas decreases for Schmidt number *Sc* Brownian motion parameter *Nb*.

2. For $\lambda = 1.2$; velocity profile enhances with enhancement in the entries of Casson fluid parameter β, magnetic parameter *M* and non-linear stretching parameter *N*. On the other hand, fluid temperature increases with increase in Schmidt number *Sc* Brownian motion parameter *Nb*, thermophoresis parameter *Nt* and decreases with the increase of Casson fluid parameter β, magnetic parameter *M* and non-linear stretching parameter *N*. Also, concentration profile rises for thermophoresis parameter *Nt* while declines for higher values of Schmidt number *Sc*, Casson fluid parameter β, magnetic parameter *M*, non-linear stretching parameter *N* and Brownian motion parameter *Nb*.
3. Boundary layer thickness decreases with an increase in.

Present study finds great application in insulation of wires, manufacturing of tetra packs, production of glass fibers, fabrication of various polymers and plastic packs, rubber sheets etc. The quality of desired product depends on the rate stretching, external magnetic field and composition of material used.

NOMENCLATURE

u	Horizontal velocity, ms^{-1}
v	Vertical velocity, ms^{-1}
x, y	Cartesian coordinates
B	Magnetic field intensity, *T*

U	Stream velocity
T	Temperature, K
C	Concentration, Kgm^{-3}
C_w	Nanoparticle volume fraction, Kgm^{-3}
q_m	Mass flux, $Kgm^{-2}\ s^{-1}$
M	magnetic field parameter, *Tesla*
Sc	Schmidt number
Pr	Prandtl number
Nu_x	Nusselt number
Nt	Thermophoresis parameter
T_∞	Ambient temperature attained, K
Sh_x	Sheerwood number
D_B	Brownian diffusion coefficient
Nb	Brownian motion parameter, $m^2\ s^{-1}$
u_w	Stretching velocity
T_w	Temperature at the sheet, K
q_w	Hass flux, $W^{-2}\ m$
C_∞	Ambient nanoparticle volume fraction, Kgm^{-3}
D_T	Thermophoresis diffusion coefficient, $m^2\ s^{-1}$

Greek symbols

ν	Kinematic viscosity, $m^2\ s^{-1}$
β	Casson fluid parameter
σ	Electrical conductivity
λ	Outer velocity parameter
ξ	Similarity variable
ρ_f	Density of base fluid, Kgm^{-3}
$\alpha_m = \frac{k_m}{(\rho c)_f}$	Thermal diffusivity
$\tau = \frac{(\rho c)_p}{(\rho c)_f}$	Ratio of heat capacities
$\theta_0(\xi)$	Non-dimensional temperature
$\phi_0(\xi)$	Non-dimensional nanoparticle concentration

Subscripts

p	Particle
∞	Ambient condition
f	Fluid
w	Wall

Superscript

$(\,)'$	Prime denotes derivative w.r.t ξ

DATA AVAILABILITY STATEMENT

No new data were created in this study. The published publication includes all graphics collected or developed during the study.

CONFLICT OF INTEREST

The author declared no potential conflicts of interest with respect to the research, authorship, and/or publication of this article.

ETHICS

There are no ethical issues with the publication of this manuscript.

REFERENCES

[1] Crane LJ. Flow past a stretching plate. Journal of Applied Mathematics and Physics (ZAMP) 1970;21:645–7. [CrossRef]

[2] Gupta PS, Gupta AS. Heat and mass transfer on a stretching sheet with suction or blowing. Can J Chem Eng 1977;55:744–6. [CrossRef]

[3] Dutta BK, Roy P, Gupta AS. Temperature field in flow over a stretching sheet with uniform heat flux. 1985;12:89-94. [CrossRef]

[4] Yoon BB, Rao RS, Kikuchi N. Sheet stretching: A theoretical-experimental comparison. International Journal of Mechanical Sciences 1989;31:579–90. [CrossRef]

[5] Sarma MS, Rao BN. Heat transfer in a viscoelastic fluid over a stretching sheet. Journal of Mathematical Analysis and Applications 1988;222:268–75.

[6] Choi SUS, Eastman JA. Enhancing thermal conductivity of fluids with nanoparticles. ASME International Mechanical Engineering Congress and Exposition, pp. 12–17, Nov. 1995.

[7] Menni Y, Chamkha AJ, Lorenzini G, Kaid N, Ameur H, Bensafi M. Advances of nanofluids in solar collectors - A review of numerical studies. MMEP 2019;6:415–27. [CrossRef]

[8] Hayat T, Qasim M, Mesloub S. MHD flow and heat transfer over permeable stretching sheet with slip conditions. Int J Numer Meth Fluids 2011;66:963–75. [CrossRef]

[9] Anwar MI, Shafie S, Hayat T, Shehzad SA, Salleh MZ. Numerical study for MHD stagnation-point flow of a micropolar nanofluid towards a stretching sheet. Journal of the Brazilian Society of Mechanical Sciences and Engineering 2017;39:89–100. [CrossRef]

[10] Shawky HM, Eldabe NTM, Kamel KA, Abd-Aziz EA. MHD flow with heat and mass transfer of Williamson nanofluid over stretching sheet through porous medium. Microsystem Technologies 2019;25:1155–69. [CrossRef]

[11] Vajravelu K, Cannon J. Fluid flow over a non linearly stretching sheet. Applied Mathematics and Computation 2006;181:609–18. [CrossRef]

[12] Matin MH, Nobari MRH, Jahangiri P. Entropy analysis in mixed convection MHD flow of nanofluid over a non-linear stretching sheet. Journal of Thermal Science and Technology 2012;7:104–19. [CrossRef]

[13] Das K. Nanofluid flow over a non-linear permeable stretching sheet with partial slip. Journal of

the Egyptian Mathematical Society 2015;23:451-6. [CrossRef]
[14] Hayat T, Ullah I, Alsaedi A, Farooq M. MHD flow of Powell-Eyring nanofluid over a non-linear stretching sheet with variable thickness. Results in Physics 2017;7:189–96. [CrossRef]
[15] Jain S, Choudhary R. Soret and Dufour effects on thermophoretic MHD flow and heat transfer over a non-linear stretching sheet with chemical reaction. International Journal of Applied and Computational Mathematics 2018;4:50. [CrossRef]
[16] Siddheshwar PG, Mahabaleshwar US. Flow and heat transfer to a Newtonian fluid over non-linear extrusion stretching sheet. International Journal of Applied and Computational Mathematics 2018;4:35. [CrossRef]
[17] Ameur H, Vial C. Modified scaba 6SRGT impellers for process intensification: Cavern size and energy saving when stirring viscoplastic fluids. Chemical Engineering and Processing - Process Intensification 2020;148:107795. [CrossRef]
[18] Nadeem S, Haq RU, Akbar NS, Khan Z. MHD three-dimensional Casson fluid flow past a porous linearly stretching sheet. Alexandria Engineering Journal 2013;52:577–82. [CrossRef]
[19] Kameswaran PK, Shaw S, Sibanda P. Dual solutions of Casson fluid flow over a stretching or shrinking sheet. Sadhana 2014;39:1573–83. [CrossRef]
[20] Hari Krishna Y, Reddy GVR, Makinde OD. Chemical reaction effect on MHD flow of Casson fluid with Porous stretching sheet. Defect and Diffusion Forum 2018;389:100–9. [CrossRef]
[21] Abdul Hakeem A, Renuka P, Vishnu Ganesh N, Kalaivanan R, Ganga B. Influence of inclined Lorentz forces on boundary layer flow of Casson fluid over an impermeable stretching sheet with heat transfer. Journal of Magnetism and Magnetic Materials 2016;401:354–61. [CrossRef]
[22] Murthy MK. MHD three dimensional flow of Casson fluid over an unsteady exponentially stretching sheet with slip conditions. Defect and Diffusion Forum 2018;388:77–95. [CrossRef]
[23] Poply V, Singh P, Yadav A. Stability analysis of MHD outer velocity flow on a stretching cylinder. Alexandria Engineering Journal 2018;57:2077–83. [CrossRef]
[24] Mabood F, Das K. Outlining the impact of melting on MHD Casson fluid flow past a stretching sheet in a porous medium with radiation. Heliyon 2019;5:1–17. [CrossRef]
[25] Raza J. Thermal radiation and slip effects on magnetohydrodynamic (MHD) stagnation point flow of Casson fluid over a convective stretching sheet. Propulsion and Power Research 2019;8:138–46. [CrossRef]
[26] Hamid M, Usman M, Khan Z, Ahmad R, Wang W. Dual solutions and stability analysis of flow and heat transfer of Casson fluid over a stretching sheet. Physics Letters A 2019;383:2400–8. [CrossRef]
[27] Vinita V, Poply V. Impact of outer velocity MHD slip flow and heat transfer of nanofluid past a stretching cylinder. Materials Today: Proceedings, Dec. 2019.
[28] Sobamowo MG. Thermo-fluidic parameters effects on nonlinear vibration of fluid-conveying nanotube resting on elastic foundations using homotopy perturbation method. Journal of Thermal Engineering 2018;4:2211–33. [CrossRef]
[29] Ravisankar R. Application of nanotechnology to improve the performance of tractor radiator using cu-water nanofluid. Journal of Thermal Engineering 2018;4:2188–200. [CrossRef]
[30] Abbas Z, Hayat T. Stagnation slip flow and heat transfer over a nonlinear stretching sheet. Numerical Methods for Partial Differential Equations 2011;27:302–14. [CrossRef]
[31] Dandapat B, Chakraborty S. Effects of variable fluid properties on unsteady thin-film flow over a nonlinear stretching sheet. International Journal of Heat and Mass Transfer 2010;53:5757–63. [CrossRef]
[32] Cortell R. Viscous flow and heat transfer over a nonlinearly stretching sheet. Applied Mathematics and Computation 2007;184:864–73. [CrossRef]
[33] Rana P, Bhargava R. Flow and heat transfer of a nanofluid over a nonlinearly stretching sheet: A numerical study. Communications in Nonlinear Science and Numerical Simulation 2012;17:212–26. [CrossRef]
[34] Almakki M, Mondal H, Sibanda P. Entropy generation in MHD flow of viscoelastic nanofluids with homogeneous-heterogeneous reaction, partial slip and nonlinear thermal radiation. Journal of Thermal Engineering 2020;6:327–45. [CrossRef]
[35] Pekmen Geridönmez B. Numerical simulation of natural convection in a porous cavity filled with ferrofluid in presence of magnetic source. Journal of Thermal Engineering 2017;4:1756–69. [CrossRef]